iScience

CellPress
OPEN ACCESS

Article

Predicting battery impedance spectra from 10-second pulse tests under 10 Hz sampling rate

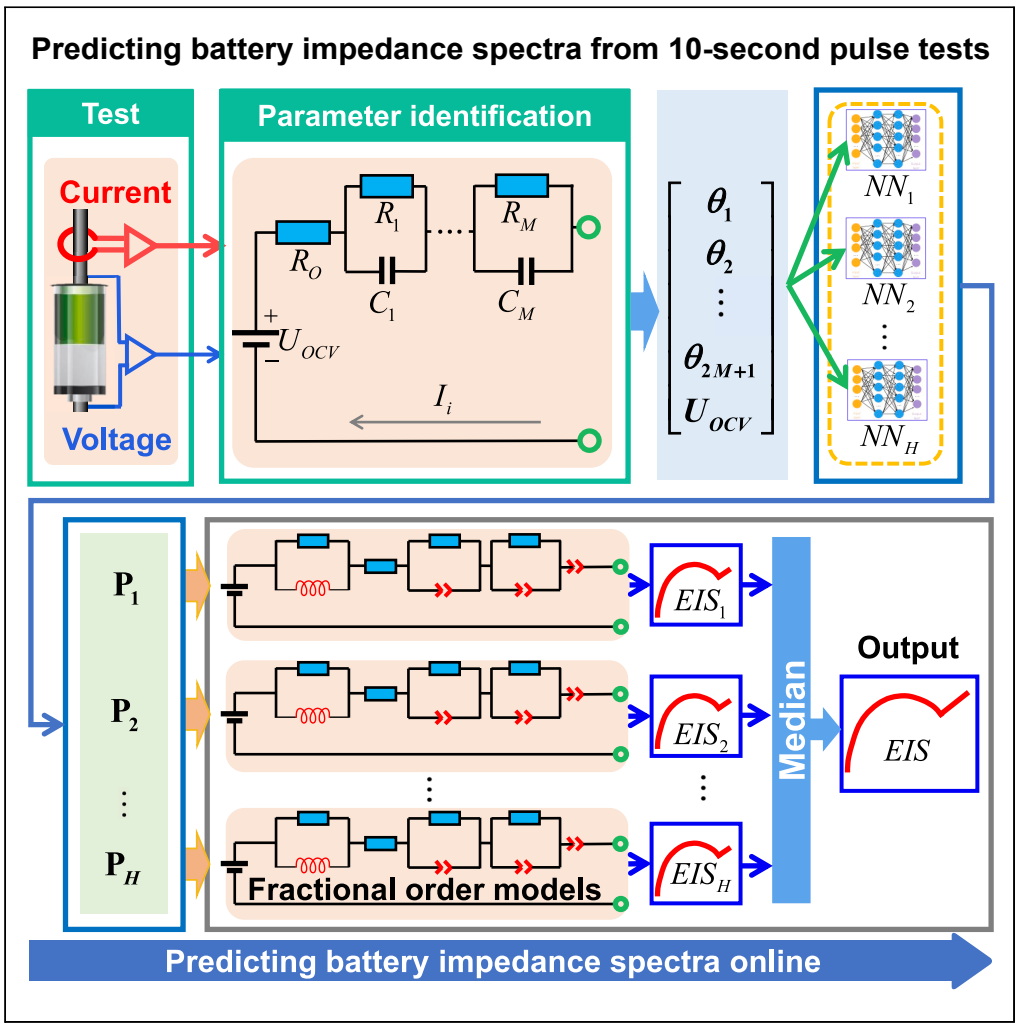

Xiaopeng Tang, Xin Lai, Qi Liu, Yuejiu Zheng, Yuanqiang Zhou, Yunjie Ma, Furong Gao

qiliu63@cityu.edu.hk (Q.L.)
kefgao@ust.hk (F.G.)

Highlights

Predict battery EIS within 10 s

The typical error is only 2 mΩ

Suitable for arbitrary dynamic load profiles

Data sampling rate is only 10 Hz

Tested with batteries under different state-of-charge and state-of-health

Tang et al., iScience 26, 106821
June 16, 2023 © 2023
https://doi.org/10.1016/j.isci.2023.106821

iScience

CellPress
OPEN ACCESS

Article

Predicting battery impedance spectra from 10-second pulse tests under 10 Hz sampling rate

Xiaopeng Tang,[1,5] Xin Lai,[1,2,5] Qi Liu,[3,6,*] Yuejiu Zheng,[2] Yuanqiang Zhou,[1] Yunjie Ma,[2] and Furong Gao[1,4,*]

SUMMARY

Onboard measuring the electrochemical impedance spectroscopy (EIS) for lithium-ion batteries is a long-standing issue that limits the technologies such as portable electronics and electric vehicles. Challenges arise from not only the high sampling rate required by the Shannon Sampling Theorem but also the sophisticated real-life battery-using profiles. We here propose a fast and accurate EIS predicting system by combining the fractional-order electric circuit model—a highly nonlinear model with clear physical meanings—with a median-filtered neural network machine learning. Over 1000 load profiles collected under different state-of-charge and state-of-health are utilized for verification, and the root-mean-squared-error of our predictions could be bounded by 1.1 mΩ and 2.1 mΩ when using dynamic profiles last for 3 min and 10 s, respectively. Our method allows using size-varying input data sampled at a rate down to 10 Hz and unlocks opportunities to detect the battery's internal electrochemical characteristics onboard via low-cost embedded sensors.

INTRODUCTION

Nowadays, lithium-ion batteries (LIBs) have revolutionized today's mobile and fast-paced society by powering portable electronics and electric vehicles. However, as with many new electrochemical devices, LIBs exhibit strong frequency-dependent characteristics, which are commonly depicted by electrochemical impedance spectroscopy (EIS).[1–3] As a non-destructive approach, EIS is very useful at all stages of LIB development in both academia and industry, from initial evaluation of electrode reaction mechanisms and kinetics,[4] to quality monitoring of packed LIBs.[5] Basically, it can be used for detecting the abnormal capacity fades[2,6] and determining the battery life span.[7,8] In addition, it provides an alternative solution for discovering the internal short circuit,[9,10] predicting the internal temperature,[11,12] and mitigating the thermal runaway.[13] Therefore, EIS has been used in a broad range of applications, especially in the lab. However, in real-life applications, onboard measuring the EIS for LIBs is still a long-standing issue until today, which is mainly due to the challenges in acquiring the specified data onboard for EIS calculation, as discussed in the following. After all, the battery load profiles are highly complicated, while the frequencies of interest between the commercial battery sensors (~10 Hz) and the impedance spectroscopy (up to 10 kHz) are always unmatched.

Normally, there are several methods to obtain EIS. Among these, the most straightforward one, which has been widely adopted in impedance testers, contains three steps. First, alternating current profiles (also known as sinusoidal current profiles or AC profiles) with different frequencies are exerted on the battery of interest. Then, both the applied current and the voltage responses are measured simultaneously. Finally, the amplitude and phase of the impedance could be readily calculated by dividing the voltage over the current in the frequency domain.[14,15] Though accurate and reliable, the device to implement the above procedure is highly expensive, which significantly limits its onboard applications. On the other hand, since the frequency-sweeping AC current required in the first step is difficult to obtain onboard, an alternative method to obtain EIS is to use pulse current profiles, which also contain information on the full frequency spectrum. After measuring the current and voltage in the second step, advanced domain transferring techniques, such as wavelet transforms[16] and Fourier transforms,[17] are applied to convert the measurements into the frequency domain for capturing the impedance spectrum. However, according to the Shannon Sampling Theorem,[18] the minimum signal sampling frequency should be 20 kHz when we need to calculate

[1]Department of Chemical and Biological Engineering, Hong Kong University of Science and Technology, Clear Water Bay, Kowloon, Hong Kong SAR 999077, China

[2]School of Mechanical Engineering, University of Shanghai for Science and Technology, Shanghai 200093, China

[3]Department of Physics, City University of Hong Kong, Tat Chee Avenue, Kowloon, Hong Kong SAR 999077, China

[4]Guangzhou HKUST Fok Ying Tung Research Institute, Guangzhou, Guangdong 511458, China

[5]These authors contributed equally

[6]Lead contact

*Correspondence: qiliu63@cityu.edu.hk (Q.L.), kefgao@ust.hk (F.G.)

https://doi.org/10.1016/j.isci.2023.106821

the impedance at 10 kHz frequency. To further guarantee the noise-rejecting performance in real-life scenarios, we tend to use a sampling rate 4x to 6x higher than the frequency of interest in the industry.[19] Such a high-frequency measurement is usually unavailable in commercial battery management systems (BMSs). When using only low-frequency measurement provided by the BMS to calculate the EIS, we have to neglect large parts of cell impedance spectra usually measured up to kHz, as discussed in ref. [20]

Considering the EIS acquisition depends extremely on the specified current profile (e.g., frequency-sweeping AC current profiles or carefully designed pulse profiles) and the signal sampling rate, it is highly desirable to develop a facial and practical method that can obtain the EIS data onboard, using more general current profiles (such as those in Figure S2, where the current may change arbitrarily from case to case) and a lower sampling rate. Very recently, advances in machine learning provide us with alternative solutions to obtain EIS from the widely used constant current profiles via a deep network.[21] However, similar to most data-driven algorithms, this approach has a strict limitation on the input data – the duration of the profile (therefore, the size of the input data) has to be fixed, and the amplitude of the current is also pre-determined. Profiles that meet these requirements may not always be accessible. Furthermore, the lack of physical explanations in this kind of machine learning algorithm reduces its adaptivity to the complicated real-life battery using scenarios where the current may change from case to case. In the departure from the previous study, here, in this work, we show that by combining machine learning tools with fractional-order models that have clear physical meanings for their elements, the battery EIS can be readily predicted using size-varying datasets collected from arbitrary dynamic load profiles with a low sampling rate. We used more than 1,000 groups of dynamic load profiles generated from different batteries with different aging degrees to verify our algorithm, and our best model achieves 1.1 mΩ root-mean-squared-error (RMSE) when using 3-min dynamic profiles. Further, when using data collected within only 10 s, we can still generate reliable predictions with RMSE bounded by 2.1 mΩ, indicating that the proposed method can be easily implemented onboard. This makes the EIS more accessible to onboard applications and promotes the advanced monitoring of the batteries.

RESULTS

Predicting EIS from 3-min pulse tests

The prediction of impedance spectra using the 3-min dynamic load profiles is first evaluated. Here, the data is collected from 16 batteries with different state-of-charge and state-of-health (see Figures S1–S3 for more details). To provide an intuitive understanding, we show a typical dynamic load profile in Figure 1A; in other words, trajectories similar to the ones in Figure 1A are used to predict the battery EIS. The predicted real and minus imaginary parts against the frequency are shown in Figures 1B and 1C, respectively. The RMSE of the prediction is given in Figure 1D. As it can be seen, the maximum RMSE is bounded by 1.1 mΩ. Noting that the best accuracy that can be expected with our experimental platform (see Section S1 for details) is 1.5 mΩ, such a low error indicates that our prediction is reliable and accurate.[22] When the sampling rate is reduced to 1Hz, the accuracy could still be bounded within 2 mΩ (See Section S2, Figures S7 and S8). To better illustrate the prediction performance, we plot eight groups of results with the minimum RMSE and another eight with the largest RMSE in Figure 2 (The prediction errors of the best and worst case can be found in Table S1). It can be noted that the shapes of the EIS vary significantly with the testing cases (Full details can be found in Figures S4–S6). For instance, only one arc in the frequencies of interest can be observed when a new battery is tested in the middle SoC range (e.g., Figure 2A), but two arcs for aged batteries in the middle SoC range (e.g., Figure 2B). When aged batteries are tested in the low SoC range (e.g., Figure 2K), one arc with a long "tail" can be seen. In all these cases, the predicted results match well with the referenced values, implying the effectiveness of the proposed method (with details shown in Figures 3 and 4).

Extraction of ohmic and charge transfer resistance

The EIS contains rich battery impedance information at different frequencies, but we still tend to use the simple resistance as an indicator of battery states (e.g., state-of-health and state-of-power) in a wide range of engineering applications for simplicity. Here, the ohmic resistance is defined as the absolute value of the impedance at such a frequency that the imaginary part is equal to zero, while the charge transfer resistance is Rp in the fractional order model (FOM) (See STAR Methods section for details).

When predicting the ohmic resistance, understanding that the impedance spectra are measured in discrete frequency values, a high-order polynomial interpolating algorithm is employed to calculate the ohmic

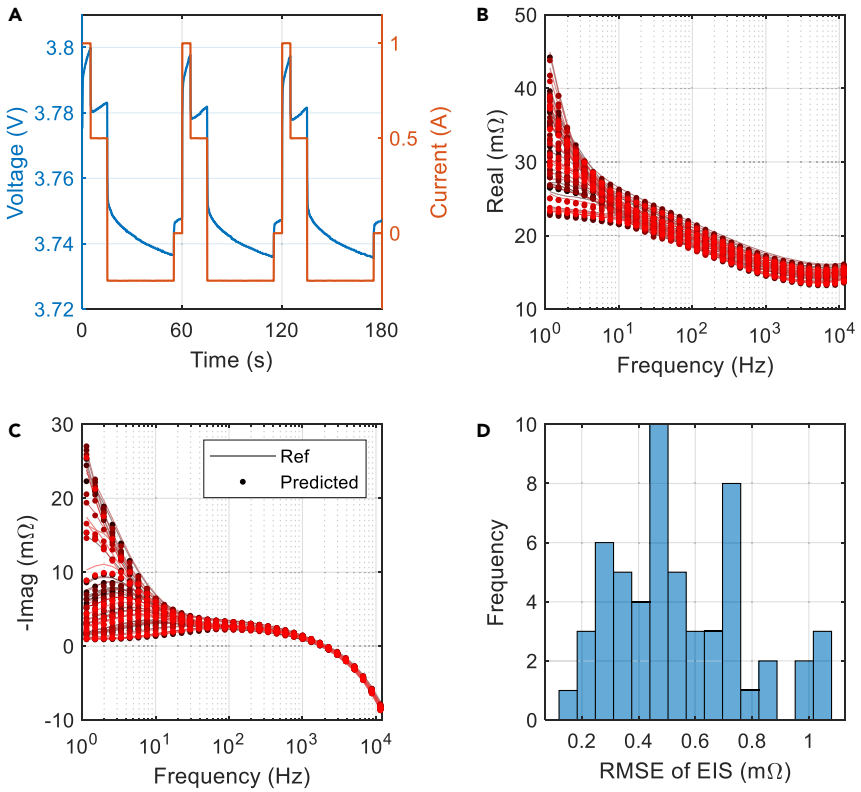

Figure 1. EIS prediction results

(A): A typical group of current and voltage data, (B): Real part, (C): Minus Imaginary part, and (D): RMSE distribution of EIS predictions. Only one group of data is shown in inset (A) for clarity, and the full dataset description can be found in supplemental information, Figure S2. In subfigures (B) and (C), different colors indicate different impedance spectra.

resistance in this work, and the results are shown in Figure 5. From Figure 5A, the predicted value matches closely with the referenced values, and most of the errors are close to zero. The RMSE of the prediction is only 0.327 mΩ, while the range of the ohmic resistance in this work is approximately 14–17 mΩ. The R^2 (coefficient of determination) is 0.7937. As illustrated in Figure 5B, all errors are bounded within ± 1 mΩ, competitive with the accuracy of our testing platform. With these results, we can conclude that the ohmic resistance can be reflected by the predicted EIS accurately.

For the charge transfer resistance, the results are shown in Figure 6. Although the RMSE of the prediction goes to 1.211 mΩ, it is worth pointing out that the range of the charge transfer resistance in this work is approximately 3–20 mΩ, much wider than the case of ohmic resistance. Here, all errors are bounded within ± 3 mΩ, and the R^2 is 0.8821, implying a high prediction accuracy.

Predicting EIS from dynamic profiles with different durations

The capability of predicting EIS from dynamic profiles with different durations is critical to meet sophisticated real-life battery-using scenarios. To scrutinize the predicting performance, we tested the proposed algorithm with nine different cases. In the first case, the dynamic profiles are truncated at the 10^{th} second so that a 100*2 vector is used as the algorithm's input when the sampling rate is 10 Hz (a 100*1 current vector and a 100*1 voltage vector). In the second to seventh cases, the duration of the dynamic load profiles are set to be 20s, 30s, 60s, 90s, 120s, and 150s, respectively. In the eighth case, the duration of the dynamic load profile is set to 10s again, but the dimensional reduction algorithm is optimized for the case with a smaller data size. To be specific, the original (100*2) vector is reduced to a (6*1) vector rather than the original (12*1) vector by changing the initial $M = 5$ to $M = 2$ in Equation 1. In this way, better noise-rejecting performance can be obtained at the cost of slightly scarifying the prediction accuracy. In the last test, a fused dataset

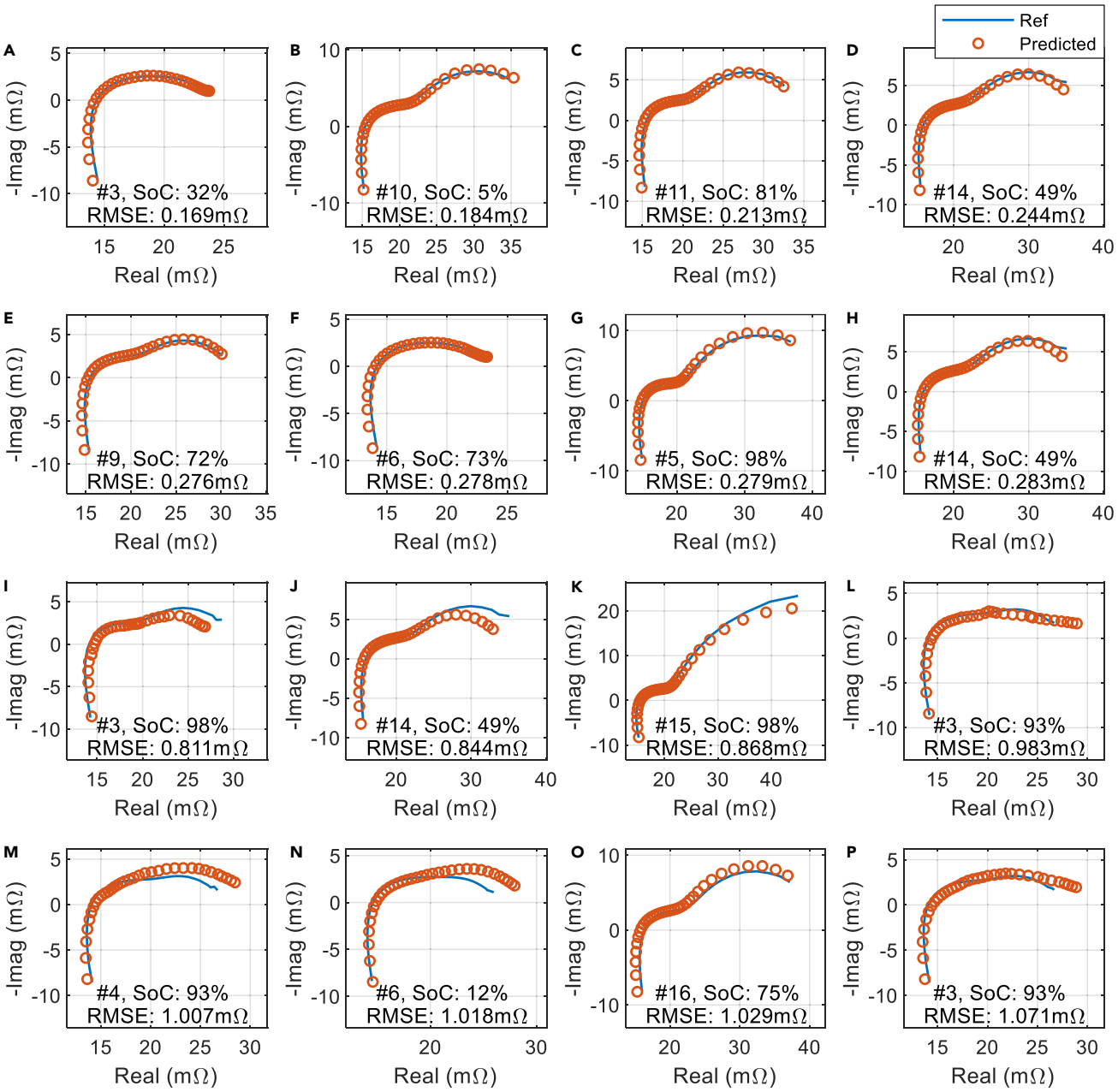

Figure 2. Nyquist plot of the EIS predictions

(A–H): eight best predictions; and (I–P): eight worst predictions. The RMSEs of the corresponding predictions are given respectively in each inset.

containing dynamic load profiles of 20s, 40s, 60s, 80s, and 100s is utilized. The distribution of the RMSE can be found respectively in Figures 7A–7I.

When the duration of the profile is longer than 20 s, all RMSE could be bounded within 3 mΩ. If the dimensional reduction algorithm is tuned for the 10-s scenario, the maximum RMSE of the prediction becomes 2.01 mΩ. When the duration of the test is longer than 60 s, the error can be generally bounded within 2 mΩ and 95% of the RMSE can be bounded within 1.5 mΩ. These results imply that fast yet accurate EIS predictions could be readily obtained from the proposed method, and a 1-min dynamic load profile could provide satisfactory predictions in most cases. Understanding the real-life battery using profiles may vary from case to case; we also test our method with the fused dataset, in which the duration of the

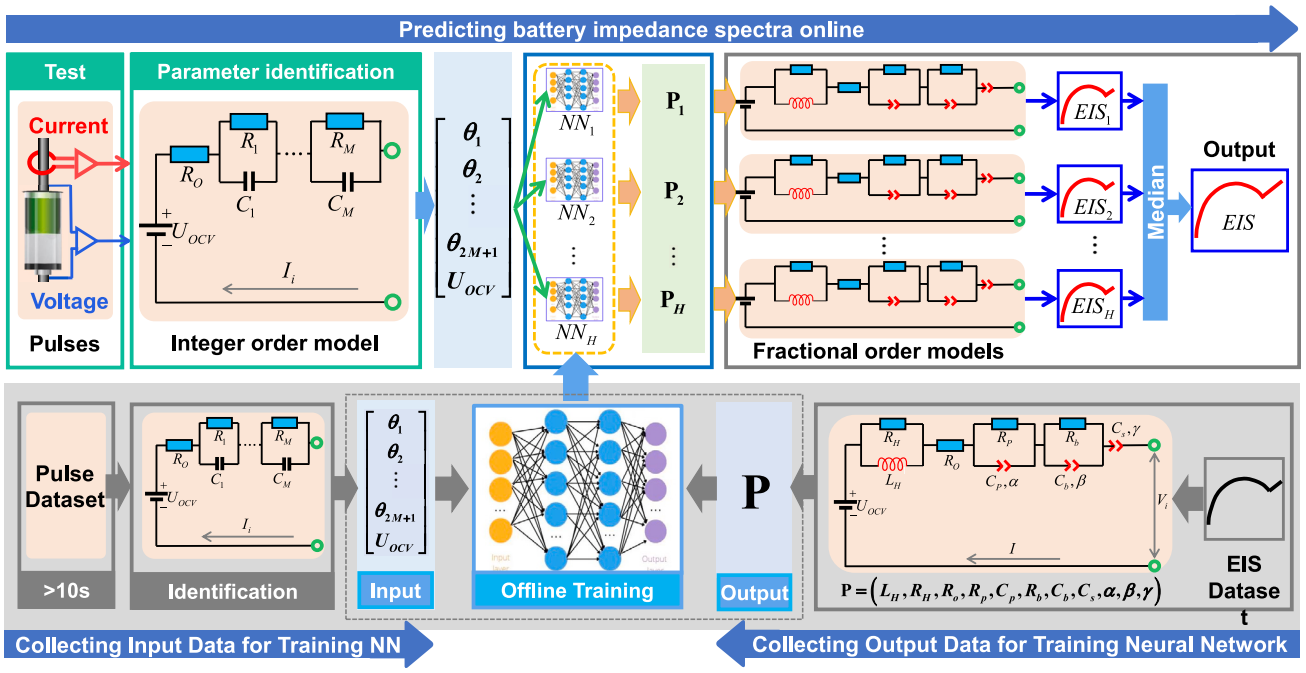

Figure 3. The framework of the proposed algorithm

profiles could change up to 500%. The RMSE of the predictions here could still be bounded within 2.2 mΩ, and 96% of the errors are lower than 1.5 mΩ. Such a low error implies the effectiveness of combining data-driven algorithms with equivalent circuit models that have clear physical meanings for each element. It also offers an effective solution to using size-varying datasets to implement data-driven-based predictions.

DISCUSSIONS

EIS is powerful for battery characterization but difficult to obtain onboard due to not only the complicated real-life battery-using scenarios but also the relatively low sampling frequency of the commercial BMSs. In this paper, we combined the machine learning tools with the fractional-order battery analysis to predict the EIS of the batteries from dynamic load profiles.

The proposed method is verified on a dataset containing more than 1,000 dynamic load profiles with different durations, patterns, state-of-charge, and state-of-health. Under a sampling rate of only 10 Hz, the EIS of up to 11.5 kHz can be accurately predicted from a dynamic load profile no longer than 3 min, and the maximum root-mean-squared error (RMSE) can be well-bounded within 1.1 mΩ. The RMSE of the ohmic resistance identified from the spectra is only 0.33 mΩ, which is close to the minimum resolution of the mainstream impedance testers (0.1 mΩ). When the length of the dynamic load profile is reduced to

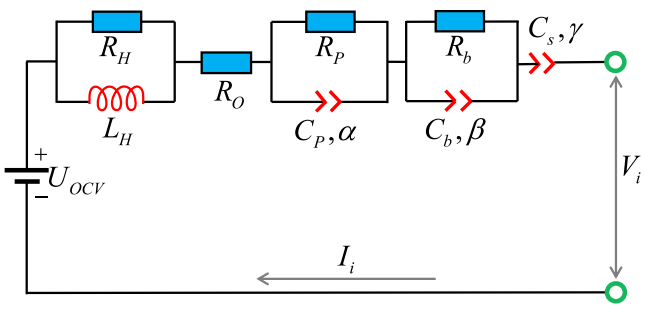

Figure 4. The employed fractional-order battery model

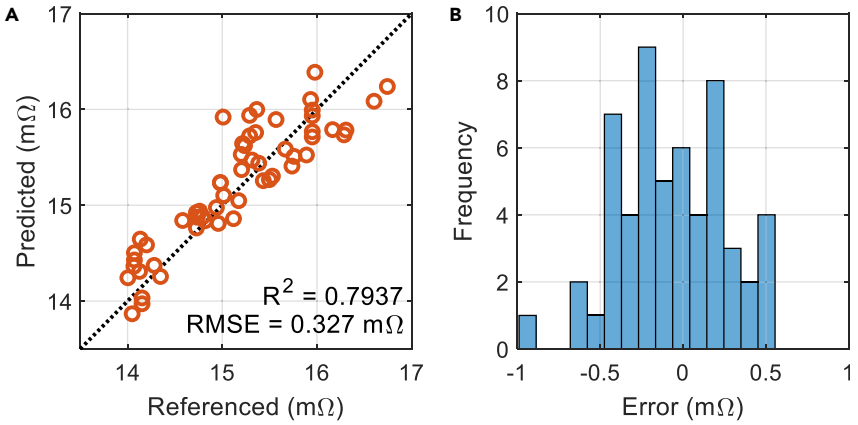

Figure 5. Prediction results of ohmic resistance
(A): Predicted values and (B): The distribution of the prediction error.

10 s, the predicted spectra could still have an RMSE lower than 2.1 mΩ, significantly improving the flexibility of the proposed method. The proposed method offers a quick and cheap approach to calculating the battery EIS onboard, which is very suitable for applications such as electric vehicles or renewable energy generation, where EIS is commonly inaccessible. It also provides an effective solution to using size-varying datasets to implement data-driven-based algorithms. This work highlights the potential of equipping machine learning tools with physical models to predict battery states under complicated conditions.

Limitations of the study

Some future works are proposed in this section to handle the limitations of the study. The temperature will be added to our model to improve the algorithm's adaptiveness to different scenarios. Approaches such as increasing the size of the dataset and widening the testing frequency can also improve the performance of our algorithm. Noise-canceling techniques will also be investigated to improve the robustness of the proposed method.

STAR★METHODS

Detailed methods are provided in the online version of this paper and include the following:

- KEY RESOURCES TABLE
- RESOURCE AVAILABILITY

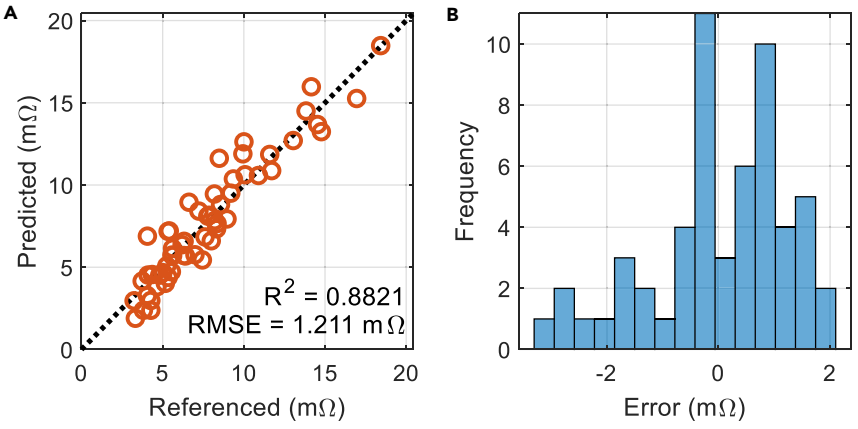

Figure 6. Prediction results of charge transfer resistance
(A): Predicted values and (B): The distribution of the prediction error.

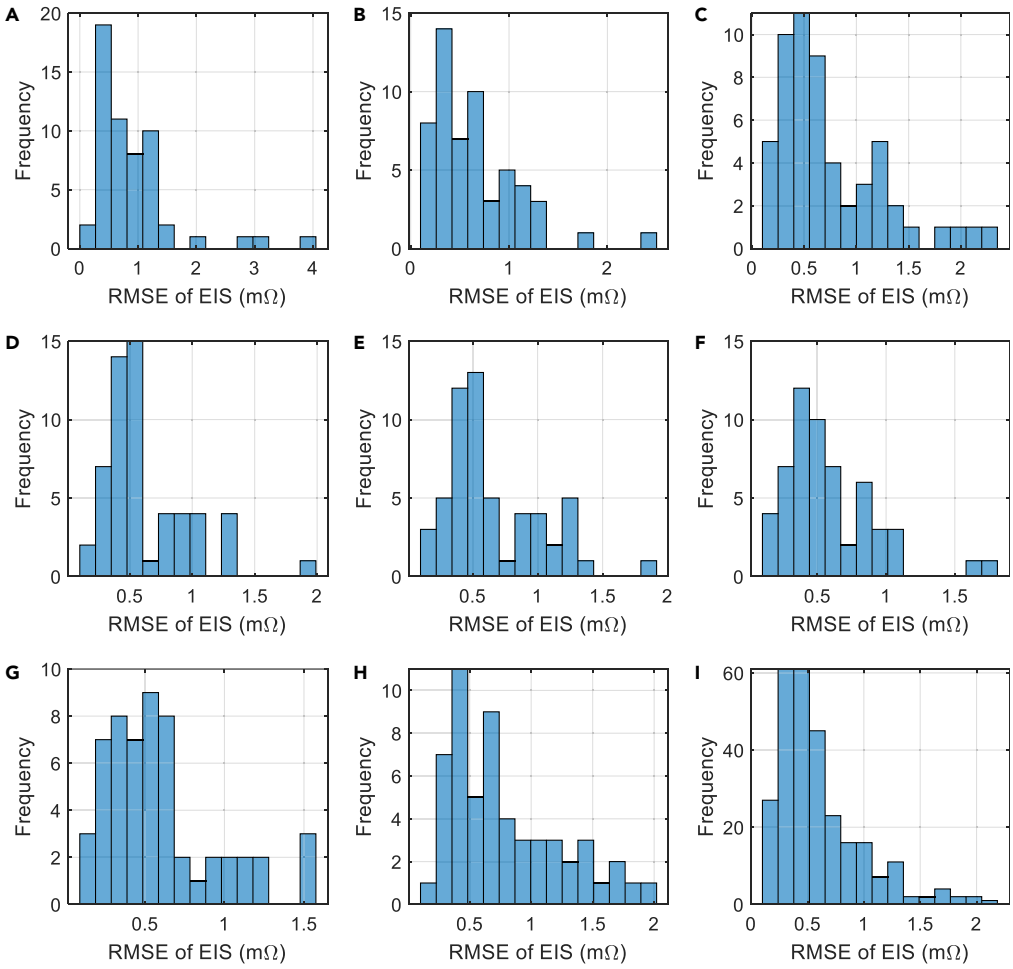

Figure 7. The distribution of the prediction errors with different testing durations

(A): Duration = 10 s, (B): Duration = 20 s, (C): Duration = 30 s, (D): Duration = 60 s, (E): Duration = 90 s, (F): Duration = 120 s, (G): Duration = 150 s, (H): Duration = 10 s (In this scenario, the original data (100*2) are reduced to the (6*1) vector, rather than the original (12*1) vector to acquire better noise rejection performance, in other words, the initial $M = 5$ is replaced by $M = 2$ in Equation 1.), and (I): Fused case, the duration includes 20, 40, 60, 80, and 100 s.

SUPPLEMENTAL INFORMATION

Supplemental information can be found online at https://doi.org/10.1016/j.isci.2023.106821.

ACKNOWLEDGMENTS

The first author would like to thank the continuing support from the Guangzhou HKUST Fok Ying Tung Research Institute during Hong Kong's unrest and the outbreak of the Covid-19.

This work is supported, in part, by the Hong Kong RGC Postdoctoral Fellowship Scheme (PDFS2122-6S06), Hong Kong Research Grant Council under grant 16208520 and 11220322, the National Natural Science Foundation of China (51977131, 52277223), the Natural Science Foundation of Shanghai (19ZR1435800),

Guangdong Scientific and Technological Project (2019A050516002), and the Foshan-HKUST Projects Program (FSUST20-FYTRI12F).

AUTHOR CONTRIBUTIONS

X. Tang and X. Lai conceived the study and developed the machine learning solution. X. Tang, Y. Zheng, and F. Gao developed the model-based solution. X. Tang and Y. Ma carried out the experiments. X. Tang and X. Lai implemented the programming and analyzed the experimental results. X. Tang, Q. Liu and X. Lai drafted the manuscript. Q. Liu, X. Lai, Y. Zhou, and F. Gao discussed the technical details, and polished the manuscript. Q. Liu and F. Gao supervised this research. All authors commented on the manuscript.

DECLARATION OF INTERESTS

We have submitted a Chinese Patent using key techniques developed in this work.

Received: February 1, 2023
Revised: April 8, 2023
Accepted: May 2, 2023
Published: May 6, 2023

REFERENCES

1. Knehr, K.W., Hodson, T., Bommier, C., Davies, G., Kim, A., and Steingart, D.A. (2018). Understanding full-cell evolution and non-chemical electrode crosstalk of Li-ion batteries. Joule *2*, 1146–1159.

2. Zhang, Y., Tang, Q., Zhang, Y., Wang, J., Stimming, U., and Lee, A.A. (2020). Identifying degradation patterns of lithium ion batteries from impedance spectroscopy using machine learning. Nat. Commun. *11*, 1706.

3. Gaberšček, M. (2021). Understanding Li-based battery materials via electrochemical impedance spectroscopy. Nat. Commun. *12*, 1–4.

4. Lu, Y., Zhao, C.-Z., Huang, J.-Q., and Zhang, Q. (2022). The timescale identification decoupling complicated kinetic processes in lithium batteries. Joule *6*, 1172–1198.

5. Díaz-González Serra Húnter Fellow, F., Heredero-Peris, D., and Galceran-Arellano, S. (2018). Design methodology for a dc–dc power conversion system with EIS capability for battery packs. Simulat. Model. Pract. Theor. *87*, 15–34.

6. Togasaki, N., Yokoshima, T., Oguma, Y., and Osaka, T. (2020). Prediction of overcharge-induced serious capacity fading in nickel cobalt aluminum oxide lithium-ion batteries using electrochemical impedance spectroscopy. J. Power Sources *461*, 228168.

7. Mc Carthy, K., Gullapalli, H., and Kennedy, T. (2022). Online state of health estimation of Li-ion polymer batteries using real time impedance measurements. Appl. Energy *307*, 118210.

8. Messing, M., Shoa, T., and Habibi, S. (2021). Estimating battery state of health using electrochemical impedance spectroscopy and the relaxation effect. J. Energy Storage *43*, 103210.

9. Xiao, F., Xing, B., Kong, L., and Xia, Y. (2021). Impedance-based diagnosis of internal mechanical damage for large-format lithium-ion batteries. Energy *230*, 120855.

10. Wang, C., Deng, T., Fan, X., Zheng, M., Yu, R., Lu, Q., Duan, H., Huang, H., Wang, C., and Sun, X. (2022). Identifying soft breakdown in all-solid-state lithium battery. Joule *6*, 1770–1781.

11. Mc Carthy, K., Gullapalli, H., Ryan, K.M., and Kennedy, T. (2021). Use of impedance spectroscopy for the estimation of Li-ion battery state of charge, state of health and internal temperature. J. Electrochem. Soc. *168*, 080517.

12. Hu, X., Feng, F., Liu, K., Zhang, L., Xie, J., and Liu, B. (2019). State estimation for advanced battery management: key challenges and future trends. Renew. Sustain. Energy Rev. *114*, 109334.

13. Srinivasan, R., Demirev, P.A., and Carkhuff, B.G. (2018). Rapid monitoring of impedance phase shifts in lithium-ion batteries for hazard prevention. J. Power Sources *405*, 30–36.

14. Firouz, Y., Relan, R., Timmermans, J., Omar, N., Van Den Bossche, P., and Van Mierlo, J. (2016). Advanced lithium ion battery modeling and nonlinear analysis based on robust method in frequency domain: nonlinear characterization and non-parametric modeling. Energy *106*, 602–617.

15. Meddings, N., Heinrich, M., Overney, F., Lee, J.-S., Ruiz, V., Napolitano, E., Seitz, S., Hinds, G., Raccichini, R., Gaberšček, M., and Park, J. (2020). Application of electrochemical impedance spectroscopy to commercial Li-ion cells: a review. J. Power Sources *480*, 228742.

16. Watanabe, H., Uemori, M., Shitanda, I., and Itagaki, M. (2022). Determination of electrochemical impedance of lithium-ion battery from charge curve by wavelet transformation. Electrochim. Acta *428*, 140957.

17. Qahouq, J.A.A., and Xia, Z. (2017). Single-perturbation-cycle online battery impedance spectrum measurement method with closed-loop control of power converter. IEEE Trans. Ind. Electron. *64*, 7019–7029.

18. Jerri, A.J. (1977). The Shannon sampling theorem—its various extensions and applications: a tutorial review. Proc. IEEE *65*, 1565–1596.

19. Alavi, S., Birkl, C., and Howey, D. (2015). Time-domain fitting of battery electrochemical impedance models. J. Power Sources *288*, 345–352.

20. Liebhart, B., Komsiyska, L., and Endisch, C. (2020). Passive impedance spectroscopy for monitoring lithium-ion battery cells during vehicle operation. J. Power Sources *449*, 227297.

21. Duan, Y., Tian, J., Lu, J., Wang, C., Shen, W., and Xiong, R. (2021). Deep neural network battery impedance spectra prediction by only using constant-current curve. Energy Storage Mater. *41*, 24–31.

22. Wang, X., Wei, X., Zhu, J., Dai, H., Zheng, Y., Xu, X., and Chen, Q. (2021). A review of modeling, acquisition, and application of lithium-ion battery impedance for onboard battery management. Etransportation *7*, 100093.

STAR★METHODS

KEY RESOURCES TABLE

REAGENT or RESOURCE	SOURCE	IDENTIFIER
Software and algorithms		
Related code	This paper	https://github.com/xtangai/iSCIENCE-D-23-00535
Related data	This paper	https://github.com/xtangai/iSCIENCE-D-23-00535

RESOURCE AVAILABILITY

Lead contact

All requests for code and data should be directed to the lead contact, Prof. Qi Liu (qiliu63@cityu.edu.hk).

Materials availability

This study did not generate new unique reagents.

Data and code availability

- The data is available online at https://github.com/xtangai/iSCIENCE-D-23-00535. In addition, the data will be shared by the lead contact upon request.
- The code is available online at https://github.com/xtangai/iSCIENCE-D-23-00535. In addition, the code will be shared by the lead contact upon request.
- Any additional information required to reanalyze the data reported in this paper is available from the lead contact upon request.

METHOD DETAILS

Data acquisition

The procedure of data acquisition can be found in the supplemental information.

Algorithm details

The overall workflow of the proposed algorithm is shown in the following Figure 3, which basically contains two parts, offline training, and online prediction. The following discussions start with the offline training part.

In the training phase, the proposed method has basically four steps: 1) Feature extraction; 2) Neural network mapping; 3) EIS reconstruction; and 4) Result enhancement.

In the first step, the key features should be extracted from the dynamic current/voltage data to reduce the cost of network training. Here, the feature extraction is implemented by identifying an integer-order electric circuit model. Denoting the obtained N-step voltage trajectory as $[V_1, V_2, \ldots, V_N]$, the corresponding current trajectory can be denoted as $[I_1, I_2, \ldots, I_N]$. Then, the battery can be modeled by the following M-order battery model ($M \ll N$, $k > M+1$):

$$D_k = [D_{k-1}, D_{k-2}, \cdots, D_{k-M}, I_k, I_{k-1}, \cdots, I_{k-M}] \cdot [\theta_1, \theta_2, \cdots, \theta_{2M+1}]^T \quad \text{(Equation 1)}$$

where $D_k = V_k - U_{OCV,k}$, and U_{OCV} stands for the open-circuit voltage, which can be approximated as a constant number during the short-term pulse test. By denoting

$$\Gamma = \begin{bmatrix} D_M & D_{M-1} & \cdots & D_1 & I_{M+1} & I_M & \cdots & I_1 \\ D_{M+1} & D_M & \cdots & D_2 & I_{M+2} & I_{M+1} & \cdots & I_2 \\ \vdots & \vdots & \vdots & \vdots & \vdots & \vdots & \vdots & \vdots \\ D_{N-1} & D_{N-2} & \cdots & D_{N-M} & I_N & I_{N-1} & \cdots & I_{N-M} \end{bmatrix} \quad \text{(Equation 2)}$$

the battery model can be identified by the total least square algorithm

$$\widehat{\Theta} = [\widehat{\theta}_1, \widehat{\theta}_2, \cdots, \widehat{\theta}_{2M+1}]^T = \left(\Gamma^T \cdot \Gamma - \sigma^2 I\right) \cdot \Gamma^T \cdot D^T_{(M+1):N} \quad \text{(Equation 3)}$$

where σ is the smallest singular value of $[\Gamma D^T_{(M+1):N}]$. Now, the original N*2 vector is reduced to a $(2M + 1)$*1 vector. In this work, $M = 5$ is recommended for the integer-order model, and the value of M may be reduced if N is small or Γ is close to ill-conditioned.

In the second step, we train a four-layer neural network that can convert the parameters in the integer-order model into the parameters of a fractional-order battery model. As illustrated in Figure 3, a neural network with $[\Theta, U_{OCV}]^T$ as input and the vector $\mathbf{P} = (L_H, R_H, R_o, R_p, C_p, R_b, C_b, C_s, \alpha, \beta, \gamma)$ as output can be readily trained, provided that sufficient training data can be acquired.

In the third step, the parameters of the FOM are readily obtained, and the impedance value (complex number) at a given frequency f can be readily calculated from $G(f)$ following Equation 4 based on the FOM described in Figure 4:

$$G(f) = \frac{L_H \cdot R_H \cdot (j \cdot 2\pi f)}{R_H + L_H \cdot (j \cdot 2\pi f)} + R_o + \frac{R_p}{1 + R_p \cdot C_p \cdot (j \cdot 2\pi f)^{\alpha}} + \frac{R_b}{1 + R_b \cdot C_b \cdot (j \cdot 2\pi f)^{\beta}} + \frac{1}{C_s \cdot (j \cdot 2\pi f)^{\gamma}} \quad \text{(Equation 4)}$$

In this way, the high-frequency response of the batteries can be calculated even if the accurate modeling parameters are obtained with low-frequency measurements.

Finally, the proposed method is tested for H times, and the median value of these H groups of results is selected as the final result to minimize the influence of noise/random network initialization.

In this paper, the identification for FOM is implemented with an enhanced Particle Swarm Optimisation algorithm offline, and the neural network is trained with a Bayesian regularisation backpropagation algorithm using more than 1000 groups of dynamic pulse profiles.

When predicting the EIS online, we first use Equation 3 to obtain the input vector for the network. Then, the input is fed into overall H parallel-connected feedforward neural networks to generate H FOMs with different parameters.

Assuming a predicted EIS trajectory contains the data sampled at L different frequencies $(f_1, f_2, \ldots, f_L)$. The root-mean-squared-error of the prediction can be calculated by:

$$RMSE = \sqrt{\frac{\sum_{i=1}^{i=L} \left(G(f_i) - r_i^{ref}\right)^2}{L}} \quad \text{(Equation 5)}$$

where r_i^{ref} stands for the referenced impedance values sampled at these L frequency points.